Research Square

Preprints are preliminary reports that have not undergone peer review.
They should not be considered conclusive, used to inform clinical practice,
or referenced by the media as validated information.

Silica-challenged macrophage secretome drives distinct alveolar and bronchial epithelial-fibroblast crosstalk: a multicellular preclinical modelling approach

Sakthi Priya Selvamani

priya.selvamani@addri.org.au

Asbestos and Dust Diseases Research Institute

Ling Zhuang

Asbestos and Dust Diseases Research Institute

Ben Johnson

Asbestos and Dust Diseases Research Institute

Ellen Donohoe

Asbestos and Dust Diseases Research Institute

Huaikai Shi

Asbestos and Dust Diseases Research Institute

Richard Zelei

Asbestos and Dust Diseases Research Institute

Vivek Dharwal

Asbestos and Dust Diseases Research Institute

Maaike Kockx

Anzac Research Institute

Caroline Reddel

Anzac Research Institute

Deborah Yates

Holdsworth House Medical Practice

Anthony Linton

Asbestos and Dust Diseases Research Institute

Elham Hosseini-Beheshti

Asbestos and Dust Diseases Research Institute

Research Article

Keywords: Silicosis, 3D spheroids, transwell, inflammation, epithelial-mesenchymal transition, fibrogenesis, extracellular matrix remodelling

Posted Date: November 4th, 2026

DOI: https://doi.org/10.21203/rs.3.rs-10872999/v1

License: This work is licensed under a Creative Commons Attribution 4.0 International License.
Read Full License

Additional Declarations: No competing interests reported.

Abstract

Background

Silicosis is an irreversible occupational lung disease that involves complex cellular mechanisms including inflammation, epithelial-mesenchymal transition (EMT), matrix remodelling, and fibrosis. Most *in vitro* studies have used conventional 2D models, which fail to orchestrate tissue architecture. While animal models have provided valuable information on silicosis pathogenesis, differences in anatomy and respiratory characteristics limit their use. With rapid advancements in 3D culture technologies, it is important to develop more physiologically relevant models to improve our understanding of silicosis.

Methods

THP-1-derived macrophages were exposed to silica nanoparticles, and their viability, cytotoxicity, and inflammatory responses were assessed by MTT assay ,LDH assay, and real-time PCR. This silica secretome was applied to alveolar and bronchial epithelial cells and fibroblasts established in 2D, 3D spheroids, and transwell models either in mono- culture or co-cultures. Cellular viability, inflammatory response, EMT, and extracellular matrix remodelling (ECM) were evaluated by CellTiter-Glo, real-time PCR, and western blotting.

Results

Silica nanoparticles induced cytotoxicity and inflammation in macrophages. Silica secretome altered cell viability and inflammatory response in 2D models of epithelial cells. Alveolar epithelial cells in 3D models showed a partial EMT transition (hybrid), while alveolar epithelial-fibroblast 3D co-culture demonstrated pronounced effects on viability, inflammation, and fibrotic remodeling compared to bronchial epithelial cells. Transwell co-cultures further revealed epithelial cell type-dependent differences in fibroblast activation.

Conclusion

These findings highlight the significance of multicellular 3D models in better reflecting key silicosis mechanisms and support their potential use as a physiologically relevant platform for mechanistic studies and therapeutic screening.

Introduction

Silicosis is a progressive and irreversible occupational lung disease caused by long-term exposure and inhalation of respirable crystalline silica particles. Silica exposure initiates persistent pulmonary inflammation, tissue scarring, dysregulation of the immune system, and matrix remodeling, which can

ultimately lead to the development of silicotic nodules and progressive lung fibrosis (1–5). Silicosis is a major global public health concern in both developed and developing countries (1, 6–10), with more than 230 million people estimated to be exposed to silica each year (11). Workers in industries such as construction, mining, quarrying, foundry, sandblasting, and tunnelling are particularly impacted by this health hazard (12).

Clinically, silicosis is broadly classified as: (i) acute – developing within a few months of intense silica exposure, (ii) accelerated – within 5 to 20 years of high-level exposure, and (iii) chronic - after 15 to 20 years of low to moderate silica exposure (13). Once established, pulmonary fibrosis may continue to progress even after exposure cessation. Currently, there is no effective treatment for silicosis. While oral prednisolone improved lung function in a small cohort of patients with silicosis, they pose a risk for the development of tuberculosis (14, 15). Drugs such as nintedanib and pirfenidone demonstrated anti-fibrotic effects in idiopathic pulmonary fibrotic disease, offering promising potential for silicosis research and treatment (16–19).

Alveolar macrophages (AMs), which act as the primary immune responder, play a vital role in silicosis (13). They engulf silica particles, leading to reactive oxygen species (ROS) production and inflammasome activation. Subsequently, they undergo apoptosis and release various factors essential for inflammatory and fibrotic processes (20–22). These factors contribute to the recruitment of other immune cells, leading to sustained inflammation, thereby damaging epithelial cells, fibroblasts, and other cells in the environment (21). The persistent damage by silica leads to epithelial-mesenchymal transition (EMT) and accelerates fibroblast activation and extracellular matrix (ECM) remodeling (21, 23). To better understand the complex multicellular crosstalk involved in the progression of silicosis and test the efficacy of anti-fibrotic drugs, an appropriate platform that more accurately reflects human pathophysiology is vital.

Several studies, either *in vitro* or *in vivo*, or a combination of both, have been conducted to investigate the effects of silica particles on pulmonary disease mechanisms and therapeutic evaluation. Animal models such as mice and rats, and cell culture models consisting of alveolar and bronchial epithelial cells, fibroblasts, and macrophages derived from both human and animal sources, are widely used to study silica pathogenesis (23–28). While most studies have focused on either one or more cell types derived from the above-mentioned sources to elucidate silica disease mechanisms, very few investigations have been carried out to evaluate multicellular crosstalk among different cells involved in silicosis (29, 30). Silicosis research in animal models is essential to simulate the inhalation route, assess lung function, monitor dosing toxicity, and investigate mechanistic disease pathways. However, these models inadequately reflect silicosis disease mechanisms observed in humans owing to differences in animal gender, genetics, anatomy, respiratory parameters, and aerosol distribution (31–34).

While two-dimensional (2D) cell culture models have shed light on the pathogenesis of silicosis (35–37), their limitations include poor representation of human physiological settings, variable patterns in cell growth, morphology, and functions that hinder their ability to model silicosis progression and

multicellular crosstalk (30, 38–41). Several three-dimensional (3D) cell culture models that closely mimic the real tissue architecture, spatial arrangement, and behavior have emerged, enabling researchers to bridge the gap between the conventional 2D and animal models (42–44). Notable advancements and diverse engineering techniques have allowed researchers to select the 3D model that best fits their scientific question and have gained popularity to evaluate silica-induced disease conditions (32, 40, 42).

In this study, we investigate the macrophage-epithelial-fibroblast crosstalk in silicosis using complementary human cell culture platforms that differ in cellular composition and spatial organization. We previously established a 3D spheroid model to demonstrate its effectiveness in understanding cellular mechanisms underpinning treatment resistance in pleural mesothelioma (45, 46). We utilized 2D and 3D spheroid systems incorporating human alveolar (A549) and bronchial (BEAS-2B) epithelial cells, together with human lung fibroblasts (MRC5), to examine the effects of macrophage-mediated signaling following silica exposure. These preclinical models were exposed to silica-challenged THP-1-derived macrophage secretome to evaluate the impact of immune cell-driven signaling on cell viability, inflammation, EMT phenotype, and ECM remodeling to determine how multicellular interactions and spatial distribution influence silica-induced phenotypes. This study provides insights into macrophage-mediated signaling and multicellular crosstalk in silicosis pathogenesis and highlights the importance of model architecture when developing human-relevant platforms for mechanistic investigation and therapeutic screening.

Materials and Methods

Cell Culture

Human lung adenocarcinoma epithelial cell line A549 (ATCC, USA) and human embryonic lung fibroblast cell line MRC5 (ATCC, USA) were cultured in RPMI 1640 media (Thermo Fisher Scientific, #11875093) supplemented with 10% fetal bovine serum (FBS) (Bovogen, #SFBS). The human monocyte cell line THP-1 (Tohoku Hospital Pediatrics) purchased from ATCC was cultured in RPMI 1640 with 10% FCS and 0.05 mM β-mercaptoethanol (Gibco, #21985023). THP-1 cells were differentiated to macrophages by treating with 50 µg /ml PMA (Sigma Aldrich, #P8139) and β-mercaptoethanol for 72 h. Human bronchial epithelial cells BEAS-2B (ATCC, USA) were grown in Bronchial Epithelial Cell Growth Medium (Lonza Bioscience, #CC-3170) in tissue culture flasks pre-coated with 10 µg/mL BSA (Sigma Aldrich, #A8806) and 30 µg /mL type I bovine collagen (Sigma Aldrich, #804592) overnight, as per the recommendations of ATCC. All cells were maintained in a 5% CO_2 incubator at 37°C.

Silica treatment of macrophages

11 nm (Sigma Aldrich, #381276) and 500 nm (Sigma Aldrich, #805890) sized silica particles commercially purchased were suspended in MilliQ water to a final concentration of 10 mg/mL and stored at 4°C. 5 x 10^5 THP-1 monocytes were plated in each well of a 6-well tissue culture plate to

differentiate into macrophages and treated with 11 nm silica particles (6.25 μg/cm^2) in 2 mL of RPMI media with no β-mercaptoethanol for 96 h. The cell culture supernatant, hereafter referred to as conditioned media (CM), was collected, centrifuged at 2000 x g for 10 min, transferred to a fresh tube, and stored at -80°C until further use. For control CM, differentiated macrophages were replaced with normal growth medium, with no β-mercaptoethanol.

MTT and LDH assay

Macrophages were plated in a 96-well tissue culture plate and treated with 11nm and 500nm silica (6.25 and 12.5 μg/cm^2) from 24 to 96 h. Cell viability for each time point was determined by MTT assay by adding 3-(4,5-dimethylthiazol-2-yl)-2,5 diphenyltetrazolium bromide solution (Invitrogen, #M6494) to a final concentration of 5 μg /mL and incubated for 2 h in a 37°C incubator. Next, the media was removed, 50 μL DMSO was added to each well to solubilise the formazan crystals, and the absorbance was measured at 540 nm. Cytotoxic effects of silica, determined by the release of lactate dehydrogenase (LDH), were measured by LDH assay (Abcam, #ab6593) as per the manufacturer's instructions. The untreated cells were lysed to measure maximal LDH release, serving as the positive control.

2D cell culture

For 2D models, A549 and BEAS-2B epithelial cells were plated in 6-well plates at densities of 1×10^5 and 2×10^4 for the Day 3 and Day 7 time points in 2 mL of corresponding cell culture medium, respectively.

3D monoculture and co-culture spheroids

For monoculture spheroids, 2500 epithelial cells were plated in 100 μl of corresponding cell culture medium per well in an ultra-low attachment (ULA) 96-well round-bottom plate (Costar, #7007). For co-culture spheroids, epithelial cells and fibroblasts were seeded in each well at a density of 2500 cells/100 μL in a 2:1 ratio. The plate was centrifuged at 300 × g for 15 min and placed in a 5% CO2 incubator at 37°C for 3 days to allow spheroid formation. The spheroids were imaged in a phase contrast microscope from Leica Microsystems (DMi 1) with a 10X objective. Images were captured at 72 h after plating (Day 0), and 3 and 7 days post silica CM exposure, and the spheroid diameter was measured by ImageJ software.

Transwell culture

The fibroblasts were seeded into the lower chamber of the 6-well or 12-well plate in RPMI media and placed at 37°C overnight. Transwell inserts with a 0.4 μm pore size (polyester membrane, Costar #3450 or #3460) were hydrated with the corresponding cell culture media for 1 h at 37°C, followed by coating with 10 μg/mL BSA and 30 μg /mL type I bovine collagen for 1 h at 37°C. Next, the epithelial cells were

seeded onto the transwell inserts. The next day, the transwell inserts seeded with epithelial cells were assembled with fibroblasts, followed by CM treatment.

Conditioned media treatment

All the models were treated with control and silica CM in a 1:1 ratio with appropriate cell culture media. For the Day 7 time point, the media was replenished with fresh CM after 3 days of initial treatment. Cells were harvested on Day 3 and Day 7 post-treatment, respectively.

Viability assay

The viability of cells after CM treatment across all cell culture models was determined by ATP quantification, which indicates the availability of metabolically active cells. For 2D and transwell cultures, the CellTiter-Glo® 2.0 Assay (Promega, #G9241) and for 3D spheroids mono- and co-cultures, the CellTiter-Glo® 3D Cell Viability Assay (Promega, #G9681) was used following the manufacturer's protocol. The luminescence was measured in a FLUOstar Omega microplate reader (BMG LabTech, Germany), and viability was determined as a percentage (%) intensity relative to the control.

RNA isolation and cDNA preparation

RNA isolation from the harvested cells was performed using the Total RNA purification kit (Norgen Biotek Corp, #SKU 17250) as per the manufacturer's protocol and quantified using the Nanodrop spectrophotometer (Thermofisher Scientific). An equal amount of RNA was reverse transcribed using the iScript™ cDNA synthesis kit (BioRad, #1708891) with the following thermal cycler conditions: 5 min at 25°C, 20 min at 46°C, and 1 min at 95°C. The cDNA was stored at -20°C until further use.

Real-time PCR

Real-time PCR was performed using KAPA SYBR® FAST kit (Sigma-Aldrich, #KK4618) in a ViiA7 Real-Time PCR System (Applied Biosystems) with the following thermal conditions: 95°C for 10 min, 95°C for 15 s, 60°C for 20 s. Normalization of each gene expression was relative to the housekeeping gene (β-actin), and fold change was calculated relative to the control using the double-delta C_t method. Gene-specific primers were purchased from Integrated DNA Technologies or Sigma-Aldrich.

Western blot

Cell lysates were prepared using Pierce™ RIPA buffer (Thermo Scientific, #89901) supplemented with protease (Sigma-Aldrich, #11836170001) and phosphatase (Sigma-Aldrich, #4906845001) inhibitor cocktails. Protein estimation was performed using Pierce™ BCA Protein Assay Kit (ThermoFisher Scientific, #23225). Equal amounts of protein were mixed with 6 x gel loading buffer and denatured at

100°C for 5 min. The proteins were loaded onto an appropriate percentage of SDS-PAGE and electrophoresed at 80 to 90 V for 1.5 to 2 h in 1 X SDS-PAGE running buffer and transferred to a PVDF (polyvinylidene fluoride) membrane for 2 h at 100 V, 4°C. Blocking of the PVDF membrane was performed in 5% BSA (bovine serum albumin) solution prepared in 1 x TBST (Tris-buffered saline, 0.1% Tween 20) for 1 h and incubated with the appropriate primary antibody (1:2000 dilution) at 4°C overnight. The following day, the membrane was washed thrice with 1 X TBST (5 minutes each), incubated with the corresponding secondary antibody (1:10,000 dilution) for 1 h at room temperature, washed thrice with 1 X TBST (5 minutes each), and imaged in a Bio-Rad ChemiDoc™ MP imaging system. The intensity of the bands was quantified using ImageJ software. A list of antibodies is available in Supplementary Table 1.

Statistical analysis

GraphPad Prism v10.6.1 was used for computing statistical analyses, and all data are presented as mean ± SEM. For time course experiments involving multiple groups, two-way ANOVA was used, followed by Dunnett's multiple comparison test for post hoc pairwise analysis. The significance of two independent groups was determined by a two-tailed unpaired Student's t-test. A p-value less than 0.05 is considered statistically significant. Significance of data is presented as * $p < 0.05$, ** $p < 0.01$, *** $p < 0.001$, and **** $p < 0.0001$.

Results

1. Silica nanoparticles induce cytotoxicity and inflammation in macrophages

The toxic effects and immunogenic potential of silica nanoparticles (11 nm and 500 nm) were evaluated in THP-1 cells. Cell viability, cytotoxicity, and expression profile of inflammatory cytokines were analyzed over 96 h. Across all time points, silica treatment with both sizes did not affect cell viability, though 11 nm silica induced a minor reduction in cell viability in a dose- and time-dependent manner, as determined by the MTT assay (Fig. 1B). The size-dependent disparity revealed the cytotoxic effects induced by silica nanoparticles, as elucidated by the LDH release assay. 11 nm silica exhibited pronounced cytotoxic effects compared to 500 nm in a time- and dose-dependent manner (Fig. 1C). To further investigate the mechanistic impact of the macrophage-derived silica CM, on epithelial and fibroblast cells, a sub-toxic dose (6.25 µg/cm2) of 11 nm silica for 96 h exposure on macrophages was chosen for further experiments. Exposure to 11 nm silica particles for 96 h triggered an inflammatory profile in THP-1 cells relative to control. Real-time PCR (Fig. 1D) showed elevated levels of pro-inflammatory cytokines, including TNF-α, IL-6, IL-1β, and TGF-β, and IL-8 chemokine.

2. Silica-challenged macrophage secretome alters cell viability and inflammation in a 2D model of A549 and BEAS-2B cells

The effects of silica CM on alveolar epithelial (A549) and bronchial epithelial (BEAS-2B) cells were assessed when cultured in conventional 2D cell culture models. A cell viability assay determined silica-induced toxicity. Exposure to silica CM significantly reduced A549 cell viability on Day 3, with partial

recovery on Day 7 (Fig. 2B). BEAS-2B cells showed a contrasting response, with no change in cell viability on Day 3 (Fig. 2C) and a mild increase on Day 7 in response to CM.

The inflammatory response to CM was determined by measuring IL-6 mRNA levels. When exposed to silica CM, A549 cells exhibited elevated inflammation on Day 3 that continued to increase until Day 7 (Fig. 2D), demonstrating both acute and chronic inflammation. Although IL-6 spiked on Day 3 in BEAS-2B (Fig. 2E), its level dropped significantly on Day 7, indicating an acute inflammatory phase rather than a chronic one. The mRNA profile of epithelial-mesenchymal transition (EMT) markers in A549 cells (Fig. 2F) exposed to silica CM demonstrates a reduction in the epithelial marker E-cadherin across both time points, an increase in the mesenchymal markers N-cadherin and vimentin, as well as the EMT transcription factor SNAI2, commonly known as SLUG, specifically on Day 7. When exposed to silica CM, BEAS-2B cells show a drastic reduction in E-cadherin on Day 7, followed by suppressed N-cadherin and SLUG, while exhibiting elevated vimentin on Day 7 (Fig. 2G).

Unlike the mRNA expression profile, the changes at the protein levels were subtle. Supplementary Fig. 1 shows the protein expression profile (western blot and densitometry quantification) of EMT markers in A549 (**Supplementary Fig. 1A and 1B**) and BEAS-2B cells (**Supplementary Fig. 1C and 1D**) when exposed to silica CM in 2D models.

3. Silica induces an EMT phenotype in the 3D spheroids of A549

The effects of silica CM on A549 and BEAS-2B cells cultured in 3D spheroids were assessed. When treated with silica CM, 3D spheroids of A549 (Fig. 3B) showed a progressive decline in cell viability from Day 3 to Day 7. In BEAS-2B cells (Fig. 3C), there was an elevation of viability on Day 3, followed by a slight decrease, with almost 90% of the cells being viable on Day 7. In both A549 (Fig. 3D) and BEAS-2B (Fig. 3E), there was a marked upregulation of IL-6 on both Day 3 and Day 7, while it was statistically significant on Day 7 compared to the control. This elevation was relatively higher in the 3D spheroids of A549 compared to BEAS-2B cells. To determine if silica exposure drives a pro-fibrotic phenotype in the epithelial cells, EMT markers were assessed both at mRNA and protein expression levels. In A549 3D spheroids (Fig. 3F), E-cadherin was elevated on both Day 3 and Day 7. Simultaneously, the mesenchymal markers, N-cadherin and vimentin, and the transcription factor SNAI2 were all upregulated at both time points, suggesting a partial or hybrid EMT phenotype. Protein expression levels of EMT markers assessed by Western blot (Fig. 3H) and subsequent densitometry analysis (Fig. 3I) revealed a significant elevation of vimentin on Day 7 of silica-exposed A549 cells compared to control cells. Similar to A549, 3D spheroids of BEAS-2B (Fig. 3G) showed high mRNA expression of E-cadherin, N-cadherin, vimentin, and SNAI2 when exposed to silica CM for 7 days, whereas their protein levels (Fig. 3J and 3K) were unchanged. The 3D spheroids at each time point were imaged to measure their size. There were no significant changes in the spheroid sizes of both A549 and BEAS-2B except for a mild reduction at Day 7 in silica CM-exposed spheroids of both epithelial cells, as shown in **Supplementary Fig. 2A and 2B**.

4. A549 3D co-culture model shows a pronounced cytotoxic and inflammatory response to silica CM compared to BEAS-2B

Following the 3D monoculture spheroid model, we next investigated the silica CM-induced differential profile in A549 and BEAS-2B epithelial cells co-cultured with MRC5 fibroblasts. These 3D spheroids were treated with silica CM, as in the 3D monoculture model. 3D co-cultures of A549 (Fig. 4B) showed a marked decline in cell viability from Day 3 to Day 7, whereas BEAS-2B co-cultures (Fig. 4C) remained slightly higher than the control. A robust increase in inflammatory response, characterized by elevated levels of IL-6, IL-8, and IL-1β, was observed in 3D co-cultures of A549 during both acute and chronic CM exposure (Fig. 4D). IL-6 levels increased in BEAS-2B 3D co-cultures, with a significant elevation on Day 7, although this level was lower than in A549 (Fig. 4E). While E-cadherin, N-cadherin, and SNAI2 showed modest upregulation in A549 3D co-cultures during chronic exposure to silica CM, the mesenchymal marker vimentin was significantly elevated (Fig. 4F). Similarly, BEAS-2B co-cultures showed a non-significant trend towards EMT during chronic exposure, though not statistically significant (Fig. 4G). Protein expression levels of EMT markers were comparable to control in both A549 and BEAS-2B 3D co-culture models, as shown in **Supplementary Fig. 3**.

5. Fibrotic remodeling is enhanced in A549 3D co-culture model upon silica CM exposure

Subsequently, both epithelial 3D co-culture models were assessed for fibrogenesis and tissue remodeling upon exposure to silica CM. A marked upregulation of TGF-β was observed in the A549 3D co-culture model (Fig. 5A). The mRNA expression levels of fibronectin, MMP2, and TIMP2 continued to increase from Day 3 to Day 7. While collagen III, α-SMA, and PDGF-β levels had an upward trend with silica CM exposure, their levels remained relatively similar at both time points. In 3D co-cultures of BEAS-2B, the levels of TGF-β, collagen III, and fibronectin showed an increasing trend during chronic exposure to silica CM, which did not attain statistical significance (Fig. 5D). While MMP2 and TIMP2 levels were similar to control levels, α-SMA decreased from Day 3 to Day 7. Western blot analysis revealed a trend in elevation of Fibroblast activation protein (FAP) in A549 3D co-cultures during chronic exposure to silica CM (Fig. 5B and 5C). On the other hand, in BEAS-2B 3D co-cultures, while the protein expression levels of FAP were unaltered, there was a significant upregulation of fibronectin levels (Fig. 5E and 5F). As shown in **Supplementary Fig. 2C and 2D**, respectively, images of 3D spheroids of A549-MRC5 showed a mild, non-significant reduction in their size compared to BEAS-2B-MRC5 during silica CM exposure.

6. Silica CM induces an inflammatory response in both epithelial and fibroblast transwell co-cultures

A transwell co-culture model that facilitates paracrine signaling was established to assess the effects of silica nanoparticles on the epithelial and fibroblast cells. The epithelial cells (A549 or BEAS-2B) were plated on the apical membrane of the insert, and the fibroblasts on the basal chamber of the transwell setup. Silica exposure caused distinct cell-specific responses in viability. A549 cells showed a reduction in cell viability during acute exposure that mostly recovered by Day 7. The MRC5 fibroblasts co-cultured with A549 showed stable cell viability on Day 3, with a proliferative trend on Day 7 (Fig. 6B). BEAS-2B (apical) showed no significant changes in viability, while its paired MRC5 (basal) had a proliferative trend (Fig. 6C). A significantly elevated and progressive inflammatory response was observed in A549 cells during both acute and chronic exposure to silica CM (Fig. 6D). While BEAS-2B showed an elevation of IL-

6 on Day 3, its levels resolved towards baseline by Day 7 (Fig. 6E). Paracrine signaling from the epithelial cells and silica CM on the apical side induced a strong inflammatory response in the unexposed fibroblasts in the basal compartment. MRC5 co-cultured with A549 demonstrated a significant elevation of inflammatory factors such as IL-6, IL-8, and IL-1β during both acute and chronic exposure (Fig. 6F). Similarly, MRC5 co-cultured with BEAS-2B showed robust inflammation during treatment with silica CM on both Day 3 and Day 7 (Fig. 6G). While the inflammation was elevated in both the fibroblast – epithelial co-culture models, their levels dropped by Day 7 in comparison to Day 3, albeit at elevated levels compared to control. Both epithelial cells on the apical side were assessed for EMT. There was a non-significant increase in mRNA levels of SNAI2 in both A549 (**Supplementary Fig. 4A**) and BEAS-2B (**Supplementary Fig. 4D**) cells during acute exposure to silica CM, while the other mesenchymal markers remained similar to control, shown in **Supplementary Fig. 4**. Similarly, a mild trend in the increase of N-cadherin and vimentin protein levels was observed in BEAS-2B cells.

7. Fibrogenesis is promoted in fibroblasts co-cultured with both epithelial cells in a transwell model

Transcript levels of TGF-β, an upstream trigger of tissue remodeling, were quantified by real-time PCR in the fibroblasts on the basal side of both epithelial cells after exposure to silica CM. Paracrine signaling from both A549 and BEAS-2B cells induced TGF-β activation in fibroblasts during both acute and chronic exposure (Fig. 7A and 7D). Transition of fibroblasts to myofibroblasts by paracrine stimulation was assessed in fibroblast co-cultures. Western blotting and densitometry (Fig. 7B and 7C) analysis revealed similar expression of α-SMA, with a slight increasing trend in FAP, and a non-significant trend in increasing levels of fibronectin in MRC5 co-cultured with A549 that received silica CM treatment compared to control. While the levels of FAP and α-SMA were similar to baseline in fibroblasts co-cultured with BEAS-2B, there was a significant upregulation in fibronectin on Day 7 (Fig. 7E and 7F). As shown in **Supplementary Fig. 5**, an elevation in the mRNA levels of fibronectin, MMP2, TIMP2, α-SMA, and PDGF-β on Day 7 was observed in MRC5-A549 co-cultures, although they did not attain statistical significance (**Supplementary Fig. 5A**). On the other hand, mRNA levels of fibrogenesis and matrix remodeling markers were either significantly downregulated or similar to controls in MRC5-BEAS-2B co-cultures (**Supplementary Fig. 5B**).

The summary of the overall experimental workflow is represented by the graphical image in Fig. 8. Macrophages were challenged with silica for 96 h, and the obtained secretome is applied to epithelial cells and fibroblasts cultured in 2D, 3D spheroids, and transwell systems. Mechanisms of silicosis pathogenesis such as viability, inflammation, EMT, and fibrogenesis were captured during both the acute phase (Day 3) and the chronic phase (Day 7). The image was created using Biorender software.

Figure 8. Graphical abstract of workflow summary

Summary of experimental workflow and parameters assessed across various *in vitro* models when exposed to silica- challenged macrophage secretome. The image was created using Biorender (https://www.biorender.com/).

Discussion

Silica exposure induces a cascade of several cellular events that lead to irreversible and progressive lung fibrosis. Owing to various limitations of 2D cell culture and animal models, it is important to transition to 3D models. To decipher disease manifestations among various cell types involved in silicosis and to test the efficacy of therapeutics in our future studies, we incorporated macrophages, alveolar and bronchial epithelial cells, and fibroblasts, leveraging the following cell culture models: 2D monolayers and 3D spheroids for epithelial cells, 3D spheroids and transwells for epithelial-fibroblast co-cultures.

Silica particles initiate macrophage inflammation (30, 47). Our results show that even at low doses, silica nanoparticles induce direct cellular damage and inflammation. The macrophage-derived silica CM was used for downstream investigations to treat epithelial cells and fibroblasts to elucidate their effects on cell viability, EMT phenotype, fibrogenesis, and tissue remodeling. The alveolar (A549) and bronchial (BEAS-2B) epithelial cells exhibited distinct phenotypes upon treatment with macrophage-challenged silica CM. 2D models of A549 cells showed reduced cell viability and progressive inflammation, whereas BEAS-2B cell viability remained stable with resolved inflammation. Our results suggest that alveolar epithelia are more permissive to cellular alterations than the bronchial epithelium when exposed to silica-induced macrophage secretome enriched with inflammatory factors.

Damage to type II alveolar epithelial cells and their transition to EMT, causing accumulation of ECM, contributes to lung fibrosis (48, 49). Investigations on 3D spheroids revealed a more pronounced reduction in A549 viability and an inflammatory spike. The simultaneous increase in both epithelial and mesenchymal markers captures the hybrid EMT state in A549, reflecting physiological relevance and cell plasticity (50, 51). Like 2D, the viability of 3D spheroids of BEAS-2B was unaltered but exhibited both acute and chronic inflammatory responses. The observed partial EMT trend was restricted to the transcriptional level. Together, these data suggest that 3D architecture reflects physiological observations during silica exposure. Silica is deposited in the alveolar pockets when inhaled, causing damage to alveolar epithelial cells (52). The varied responses observed between alveolar and bronchial epithelial cells in our study are in alignment, suggesting that alveolar regions are the primary injury sites during silica exposure (53–55).

Silicosis pathogenesis is manifested by diverse cell types, and thus it is important to investigate the disease mechanisms in multicellular models to promote better understanding of strategies to tackle (56–58). Integrating epithelial cells and fibroblasts revealed differences in fibrogenic and matrix remodeling processes dependent on epithelial cell type. A549-MRC5 3D spheroids showed pronounced cytotoxicity, an inflammatory response, and partial EMT activation only at the transcriptional level. A significant elevation of TGF-β, with a trend towards fibroblast activation due to long-term silica CM exposure, was observed, in line with tissue remodeling processes (30, 59). On the other hand, BEAS-2B-MRC5 spheroids maintained high cell survival, an inflammatory profile similar to that of their 3D monocultures, minimal late-stage EMT activation and fibrogenesis, and a significant elevation in fibronectin levels, suggesting ECM deposition. Collectively, the differential fibrotic response between the

two epithelial cells co-cultured with fibroblasts implies variation in mechanisms specific to the epithelial lineage (60, 61).

In the transwell co-culture model, the fibroblasts on the basal side of both epithelial cells exhibited a similar high inflammatory profile and pro-fibrotic factors despite no direct contact with silica CM. This suggests that epithelial cells on the apical side induce fibroblasts through paracrine signaling by releasing pro-inflammatory factors when exposed to silica CM (43, 62). Epithelial cell-specific paracrine signals differentially regulate fibroblast activation and matrix remodeling. Being tumorigenic, factors from A549 promote fibroblast activation and transformation, while the signals from the normal bronchial epithelial BEAS-2B promote matrix remodeling by fibronectin deposition. This phenomenon is enhanced in the transwell model due to a higher density of fibroblasts compared to the 3D spheroids co-culture.

The method of spheroid generation – with or without scaffolds should be taken into consideration, as they play an important role in cellular profile and sensitivity to drugs (63). Our scaffold-free 3D spheroids demonstrate their utility for modeling multicellular inflammatory and fibrotic responses observed in silicosis. Collectively, our findings demonstrate that increasing the complexity of preclinical models reveals distinct cell survival, inflammatory, and fibrotic responses to silica-induced macrophage signalling. While monoculture models capture acute silicosis processes, co-culture systems capture epithelial-fibroblast crosstalk, supporting their utilization to reflect chronic mechanisms of silicosis progression and future therapeutic evaluation.

Limitations

A key limitation of this investigation is the use of the lung adenocarcinoma A549 cell line to represent alveolar epithelial cells (64). Limited availability, donor variability, and challenges associated with maintaining primary human type II alveolar epithelial cells restrict their use in reproducible studies. Although A549 cells originate from lung cancer, they share certain characteristics with alveolar epithelial type II cells and are widely used to model the alveolar region (65, 66). Nevertheless, findings from A549 cells should be interpreted with consideration and may not fully recapitulate the behaviour of normal human alveolar epithelium. The self-assembled 3D spheroid model provides a more spatially organized cellular environment than a conventional 2D model and can better reflect tissue architecture. However, prolonged culture can lead to the development of a hypoxic necrotic core; thus, cell density and cultivation period should be optimized to minimize this effect. Future studies incorporating more physiologically complex systems such as organoids, lung-on-chip, or perfused 3D models may improve the physiological model. Overall, the choice of cell type and 3D architecture should be guided by the research question and intended application of the model.

Conclusion

Our findings demonstrate that macrophage-derived silica secretome drives a series of cellular events including inflammation, EMT-associated phenotype, and fibrotic responses that are distinct between

alveolar and bronchial epithelial cells. Importantly, transition to 3D spheroid models reveals cellular alterations that were poorly reflected in the conventional 2D systems, highlighting the influence of spatial organisation and cellular context of the observed phenotypes. Collectively, these findings support the use of multicellular 3D models to better investigate complex cellular crosstalk underlying silicosis. Rather than viewing 3D models simply as an alternative to conventional 2D culture, our findings highlight their potential to provide complementary information on disease-associated cellular responses and to improve the physiological relevance of preclinical models. Therefore, these platforms may provide a useful foundation to understand silicosis pathogenesis and also to evaluate and screen potential therapeutics.

Abbreviations

LDH – Lactate dehydrogenase

MTT - 3-(4,5-dimethylthiazol-2-yl)-2,5 diphenyltetrazolium bromide

IL-6 – Interleukin 6

IL-8 – Interleukin 8

TNF-α – Tumour necrosis factor alpha

IL-1β – Interleukin 1 beta

TGF-β – Transforming growth factor beta

2D – Two-dimension

3D – Three-dimension

EMT – Epithelial to mesenchymal transition

ECM – Extracellular Matrix

Declarations

Acknowledgements

The authors are thankful to Kim Brislane, CEO of ADDRI, for funding acquisition, oversight, and support of this research.

Author's contributions

S.P.S – Conceptualisation, Methodology, Investigation, Formal analysis, Visualisation, Writing (original draft, review & editing). L.Z. – Investigation, Writing (review & editing). B.J. – Investigation, Writing

(review & editing). E.D. – Investigation, Writing (review & editing). H.S. – Investigation, Writing (review & editing). R.Z. – Investigation, Writing (review & editing). V.D. – Investigation, Writing (review & editing). M.K. – Resources, Writing (review & editing). C.R. - Resources, Writing (review & editing). D.Y. – Conceptualisation, Writing (review & editing). A.L. – Supervision, Project administration, Writing (review & editing). E.H.B. - Conceptualisation, Methodology, Supervision, Project administration, Writing (review & editing). All authors have reviewed the manuscript.

Funding

This work was supported by the New South Wales State Government, with oversight from the iCare Dust Diseases Board.

Availability of data

All data are available within this article and supplementary file.

Ethics approval and consent to participate

Not applicable.

Consent for publication

Not applicable.

Competing interests

All authors declare no competing interests.

References

1. Leung CC, Yu IT, Chen W. Silicosis Lancet. 2012;379(9830):2008–18.
2. Lee HL, Kim YS, Park JH, Chung WY, Lee KS, Oh YJ, et al. Selectively decreased expression of peroxiredoxins induced by silica in pulmonary epithelial cells. Korean J Intern Med. 2009;24(3):220–6.
3. Todd NW, Luzina IG, Atamas SP. Molecular and cellular mechanisms of pulmonary fibrosis. Fibrogenesis Tissue Repair. 2012;5(1):11.
4. Shin DY, Jeong MH, Bang IJ, Kim HR, Chung KH. MicroRNA regulatory networks reflective of polyhexamethylene guanidine phosphate-induced fibrosis in A549 human alveolar adenocarcinoma cells. Toxicol Lett. 2018;287:49–58.
5. Adamcakova J, Mokra D. New Insights into Pathomechanisms and Treatment Possibilities for Lung Silicosis. Int J Mol Sci. 2021;22(8).
6. Greenberg MI, Waksman J, Curtis J. Silicosis: a review. Dis Mon. 2007;53(8):394–416.

7. Tse LA, Li ZM, Wong TW, Fu ZM, Yu IT. High prevalence of accelerated silicosis among gold miners in Jiangxi, China. Am J Ind Med. 2007;50(12):876–80.
8. Nelson G, Girdler-Brown B, Ndlovu N, Murray J. Three decades of silicosis: disease trends at autopsy in South African gold miners. Environ Health Perspect. 2010;118(3):421–6.
9. Kauppinen T, Toikkanen J, Pedersen D, Young R, Ahrens W, Boffetta P, et al. Occupational exposure to carcinogens in the European Union. Occup Environ Med. 2000;57(1):10–8.
10. Mazurek JM, Attfield MD. Silicosis mortality among young adults in the United States, 1968–2004. Am J Ind Med. 2008;51(8):568–78.
11. Marrocco A, Ortiz LA. Role of metabolic reprogramming in pro-inflammatory cytokine secretion from LPS or silica-activated macrophages. Front Immunol. 2022;Volume 13–2022.
12. Hoy RF, Jeebhay MF, Cavalin C, Chen W, Cohen RA, Fireman E, et al. Current global perspectives on silicosis-Convergence of old and newly emergent hazards. Respirology. 2022;27(6):387–98.
13. Handra CM, Gurzu IL, Chirila M, Ghita I, Silicosis. New Challenges from an Old Inflammatory and Fibrotic Disease. Front Biosci (Landmark Ed). 2023;28(5):96.
14. Sharma SK, Pande JN, Verma K. Effect of Prednisolone Treatment in Chronic Silicosis. Am Rev Respir Dis. 1991;143(4Part1):814–21.
15. Venkitakrishnan R, Ramachandran D, Augustine J, Cleetus M. Inhaled corticosteroids and risk of tuberculosis-How bad is the risk? Indian J Tuberc. 2022;69(2):128–30.
16. Hostettler KE, Zhong J, Papakonstantinou E, Karakiulakis G, Tamm M, Seidel P, et al. Anti-fibrotic effects of nintedanib in lung fibroblasts derived from patients with idiopathic pulmonary fibrosis. Respir Res. 2014;15(1):157.
17. Lehmann M, Buhl L, Alsafadi HN, Klee S, Hermann S, Mutze K, et al. Differential effects of Nintedanib and Pirfenidone on lung alveolar epithelial cell function in ex vivo murine and human lung tissue cultures of pulmonary fibrosis. Respir Res. 2018;19(1):175.
18. Wollin L, Maillet I, Quesniaux V, Holweg A, Ryffel B. Antifibrotic and anti-inflammatory activity of the tyrosine kinase inhibitor nintedanib in experimental models of lung fibrosis. J Pharmacol Exp Ther. 2014;349(2):209–20.
19. Joannes A, Voisin T, Morzadec C, Letellier A, Llamas Gutierrez F, Chiforeanu DC, et al. Anti-fibrotic effects of nintedanib on lung fibroblasts derived from patients with Progressive Fibrosing Interstitial Lung Diseases (PF-ILDs). Pulmonary Pharmacol Ther. 2023;83:102267.
20. Yao SQ, Rojanasakul LW, Chen ZY, Xu YJ, Bai YP, Chen G, et al. Fas/FasL pathway-mediated alveolar macrophage apoptosis involved in human silicosis. Apoptosis. 2011;16(12):1195–204.
21. Mo S, Liu Z, Wei W, Zhang R, Xu Y. Advances in understanding the role of NLRP3 inflammasome-mediated macrophage pyroptosis in the pathogenesis of silicosis. Ecotoxicol Environ Saf. 2026;310:119811.
22. Liu TT, Sun HF, Han YX, Zhan Y, Jiang JD. The role of inflammation in silicosis. Front Pharmacol. 2024;15:1362509.

23. Xiang G, Gong L, Wang K, Sun X, Liu Z, Cai Q. Suppression of NOX2-Derived Reactive Oxygen Species (ROS) Reduces Epithelial-to-MesEnchymal Transition Through Blocking SiO(2)-Regulated JNK Activation. Toxics. 2025;13(5).
24. Ophir N, Fireman E, Kramer MR, Korenstein R. Artificial stone dust affects oxidative stress and epithelial barrier in CALU 3 cells. Exp Lung Res. 2025;51(1):81–90.
25. Rong Y, Shen Y, Zhang Z, Cui X, Xiao L, Liu Y, et al. Blocking TGF-beta expression inhibits silica particle-induced epithelial-mesenchymal transition in human lung epithelial cells. Environ Toxicol Pharmacol. 2015;40(3):861–9.
26. Liu H, Dai X, Cheng Y, Fang S, Zhang Y, Wang X, et al. MCPIP1 mediates silica-induced cell migration in human pulmonary fibroblasts. Am J Physiol Lung Cell Mol Physiol. 2016;310(2):L121–32.
27. Deshpande A, Narayanan PK, Lehnert BE. Silica-induced generation of extracellular factor(s) increases reactive oxygen species in human bronchial epithelial cells. Toxicol Sci. 2002;67(2):275–83.
28. Liang D, Wang Y, Zhu Z, Yang G, An G, Li X, et al. BMP-7 attenuated silica-induced pulmonary fibrosis through modulation of the balance between TGF-beta/Smad and BMP-7/Smad signaling pathway. Chem Biol Interact. 2016;243:72–81.
29. Li F, Song D, Meng J, Tian J, Li N, Zheng Y, et al. JunB orchestrates macrophage-fibroblast crosstalk in silica nanoparticle-induced pulmonary fibrosis. Ecotoxicol Environ Saf. 2025;303:119046.
30. Yang X, Zhang J, Xiong M, Yang Y, Yang P, Li N, et al. NF-kappaB pathway affects silica nanoparticle-induced fibrosis via inhibited inflammatory response and epithelial-mesenchymal transition in 3D co-culture. Toxicol Lett. 2023;383:141–51.
31. Martinez-Lopez A, Candel S, Tyrkalska SD. Animal models of silicosis: fishing for new therapeutic targets and treatments. Eur Respir Rev. 2023;32(169).
32. Donohoe E, Selvamani SP, Dharwal V, Zelei R, Linton A, Yates D et al. Tools of the trade: leveraging 3D in vitro models to advance silicosis research. Front Pharmacol. 2026;Volume 17–2026.
33. Ehrmann S, Schmid O, Darquenne C, Rothen-Rutishauser B, Sznitman J, Yang L, et al. Innovative preclinical models for pulmonary drug delivery research. Expert Opin Drug Deliv. 2020;17(4):463–78.
34. Seok J, Warren HS, Cuenca AG, Mindrinos MN, Baker HV, Xu W, et al. Genomic responses in mouse models poorly mimic human inflammatory diseases. Proc Natl Acad Sci U S A. 2013;110(9):3507–12.
35. Cao Z, Xiao Q, Dai X, Zhou Z, Jiang R, Cheng Y, et al. circHIPK2-mediated sigma-1R promotes endoplasmic reticulum stress in human pulmonary fibroblasts exposed to silica. Cell Death Dis. 2017;8(12):3212.
36. Qu Y, Zhai R, Wang D, Wang Z, Hou G, Wu C, et al. Mitochondrial folate pathway regulates myofibroblast differentiation and silica-induced pulmonary fibrosis. J Transl Med. 2023;21(1):365.
37. Thibodeau MS, Giardina C, Knecht DA, Helble J, Hubbard AK. Silica-Induced Apoptosis in Mouse Alveolar Macrophages Is Initiated by Lysosomal Enzyme Activity. Toxicol Sci. 2004;80(1):34–48.

38. Xue W, Wang J, Hou Y, Wu D, Wang H, Jia Q, et al. Lung decellularized matrix-derived 3D spheroids: Exploring silicosis through the impact of the Nrf2/Bax pathway on myofibroblast dynamics. Heliyon. 2024;10(13):e33585.
39. Kapalczynska M, Kolenda T, Przybyla W, Zajaczkowska M, Teresiak A, Filas V, et al. 2D and 3D cell cultures - a comparison of different types of cancer cell cultures. Arch Med Sci. 2018;14(4):910–9.
40. Jensen C, Teng Y. Is It Time to Start Transitioning From 2D to 3D Cell Culture? Front Mol Biosci. 2020;7:33.
41. Liu XQ, Kiefl R, Roskopf C, Tian F, Huber RM. Interactions among Lung Cancer Cells, Fibroblasts, and Macrophages in 3D Co-Cultures and the Impact on MMP-1 and VEGF Expression. PLoS ONE. 2016;11(5):e0156268.
42. Antoni D, Burckel H, Josset E, Noel G. Three-dimensional cell culture: a breakthrough in vivo. Int J Mol Sci. 2015;16(3):5517–27.
43. Kolanko E, Cargnoni A, Papait A, Silini AR, Czekaj P, Parolini O. The evolution of in vitro models of lung fibrosis: promising prospects for drug discovery. Eur Respir Rev. 2024;33(171).
44. Gamerith G, Rainer J, Huber JM, Hackl H, Trajanoski Z, Koeck S, et al. 3D-cultivation of NSCLC cell lines induce gene expression alterations of key cancer-associated pathways and mimic in-vivo conditions. Oncotarget. 2017;8(68):112647–61.
45. Shi H, Rath EM, Lin RCY, Sarun KH, Clarke CJ, McCaughan BC, et al. 3-Dimensional mesothelioma spheroids provide closer to natural pathophysiological tumor microenvironment for drug response studies. Front Oncol. 2022;12:973576.
46. Shi H, Selvamani SP, Zelei R, Zhuang L, Wang D, Johnson B et al. Validation of chemoresistance phenotypes in pleural mesothelioma across 2D, 3D, and in vivo models. Sci Rep. 2026;16(1).
47. Yang H, Wu QY, Li MY, Lao CS, Zhang YJ. Pulmonary Toxicity in Rats Caused by Exposure to Intratracheal Instillation of SiO2 Nanoparticles. Biomed Environ Sci. 2017;30(4):264–79.
48. Zhang Z, Qu J, Zheng C, Zhang P, Zhou W, Cui W, et al. Nrf2 antioxidant pathway suppresses Numb-mediated epithelial-mesenchymal transition during pulmonary fibrosis. Cell Death Dis. 2018;9(2):83.
49. Lamouille S, Xu J, Derynck R. Molecular mechanisms of epithelial-mesenchymal transition. Nat Rev Mol Cell Biol. 2014;15(3):178–96.
50. Rashid M, Hari K, Thampi J, Santhosh NK, Jolly MK. Network topology metrics explaining enrichment of hybrid epithelial/mesenchymal phenotypes in metastasis. PLoS Comput Biol. 2022;18(11):e1010687.
51. Liu J, Abate W, Xu J, Corry D, Kaul B, Jackson SK. Three-dimensional spheroid cultures of A549 and HepG2 cells exhibit different lipopolysaccharide (LPS) receptor expression and LPS-induced cytokine response compared with monolayer cultures. Innate Immun. 2011;17(3):245–55.
52. Merchant RK, Peterson MW, Hunninghake GW. Silica directly increases permeability of alveolar epithelial cells. J Appl Physiol (1985). 1990;68(4):1354–9.
53. Pollard KM. Silica, Silicosis, and Autoimmunity. Front Immunol. 2016;7:97.

54. Lam M, Barry KT, Hodges CJ, Harpur CM, Ong JDH, Rosli S, et al. NLRP3 deficiency abrogates silica-induced neutrophil infiltration, pulmonary damage and fibrosis. Respir Res. 2025;26(1):109.
55. Lam M, Barry KT, Hodges CJ, West AC, Harpur CM, Mansell A et al. Epithelial NLRP3 drives silica-induced lung injury and fibrosis through IL-18 and pro-fibrotic neutrophil recruitment. Part Fibre Toxicol. 2026;23(1).
56. Skuland T, Lag M, Gutleb AC, Brinchmann BC, Serchi T, Ovrevik J, et al. Pro-inflammatory effects of crystalline- and nano-sized non-crystalline silica particles in a 3D alveolar model. Part Fibre Toxicol. 2020;17(1):13.
57. Arora L, Kalia M, Dasgupta S, Singh N, Verma AK, Pal D. Development of a Multicellular 3D Tumor Model to Study Cellular Heterogeneity and Plasticity in NSCLC Tumor Microenvironment. Front Oncol. 2022;12:881207.
58. Bassi G, Grimaudo MA, Panseri S, Montesi M. Advanced Multi-Dimensional Cellular Models as Emerging Reality to Reproduce In Vitro the Human Body Complexity. Int J Mol Sci. 2021;22(3).
59. Cheng D, Xu Q, Wang Y, Li G, Sun W, Ma D, et al. Metformin attenuates silica-induced pulmonary fibrosis via AMPK signaling. J Transl Med. 2021;19(1):349.
60. Biola-Clier M, Beal D, Caillat S, Libert S, Armand L, Herlin-Boime N, et al. Comparison of the DNA damage response in BEAS-2B and A549 cells exposed to titanium dioxide nanoparticles. Mutagenesis. 2017;32(1):161–72.
61. Elje E, Mariussen E, McFadden E, Dusinska M, Runden-Pran E. Different Sensitivity of Advanced Bronchial and Alveolar Mono- and Coculture Models for Hazard Assessment of Nanomaterials. Nanomaterials (Basel). 2023;13(3).
62. Li Q, Ling Y, Ma Y, Zhang T, Yang Y, Tao S. Paracrine signaling of ferroptotic airway epithelium in crystalline silica-induced pulmonary fibrosis augments local fibroblast activation through glycolysis reprogramming. Ecotoxicol Environ Saf. 2024;271:115994.
63. Qi X, Prokhorova AV, Mezentsev AV, Shen N, Trofimenko AV, Filkov GI et al. Comparison of EMT-Related and Multi-Drug Resistant Gene Expression, Extracellular Matrix Production, and Drug Sensitivity in NSCLC Spheroids Generated by Scaffold-Free and Scaffold-Based Methods. Int J Mol Sci. 2022;23(21).
64. Lieber M, Smith B, Szakal A, Nelson-Rees W, Todaro G. A continuous tumor-cell line from a human lung carcinoma with properties of type II alveolar epithelial cells. Int J Cancer. 1976;17(1):62–70.
65. Foster KA, Oster CG, Mayer MM, Avery ML, Audus KL. Characterization of the A549 cell line as a type II pulmonary epithelial cell model for drug metabolism. Exp Cell Res. 1998;243(2):359–66.
66. Shapiro DL, Nardone LL, Rooney SA, Motoyama EK, Munoz JL. Phospholipid biosynthesis and secretion by a cell line (A549) which resembles type II aleveolar epithelial cells. Biochim Biophys Acta. 1978;530(2):197–207.

Figures

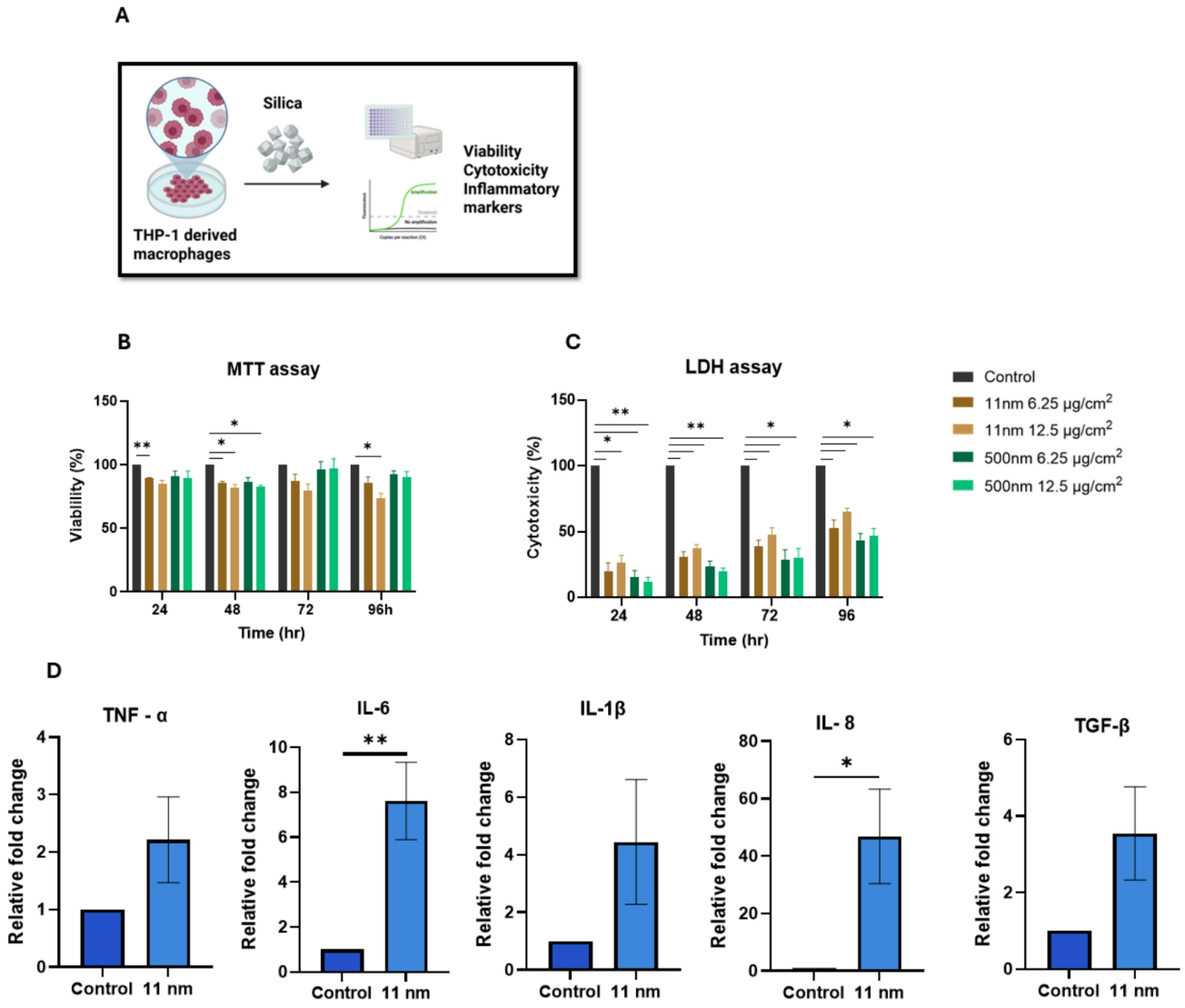


Figure 1

Silica affects cell viability, toxicity, and inflammatory profile in macrophages

(**A**) Schematic workflow. (**B**) Cell viability of THP-1-derived macrophages, assessed by MTT assay at 24, 48, 72, and 96 h after exposure to 11 nm and 500 nm silica particles at concentrations of 6.25 µg/cm^2 and 12.5 µg/cm^2, respectively. (**C**) Cytotoxicity, determined by LDH release, at the same time points and concentrations, relative to a positive control representing maximum cell lysis (100 %). (**D**) mRNA expression of inflammatory and immunomodulatory cytokines in THP-1 cells after exposure to 11 nm nanoparticles. Data are presented as the mean ± SEM (n = 5 to 6). *p < 0.05 and **p < 0.01 compared to control groups.

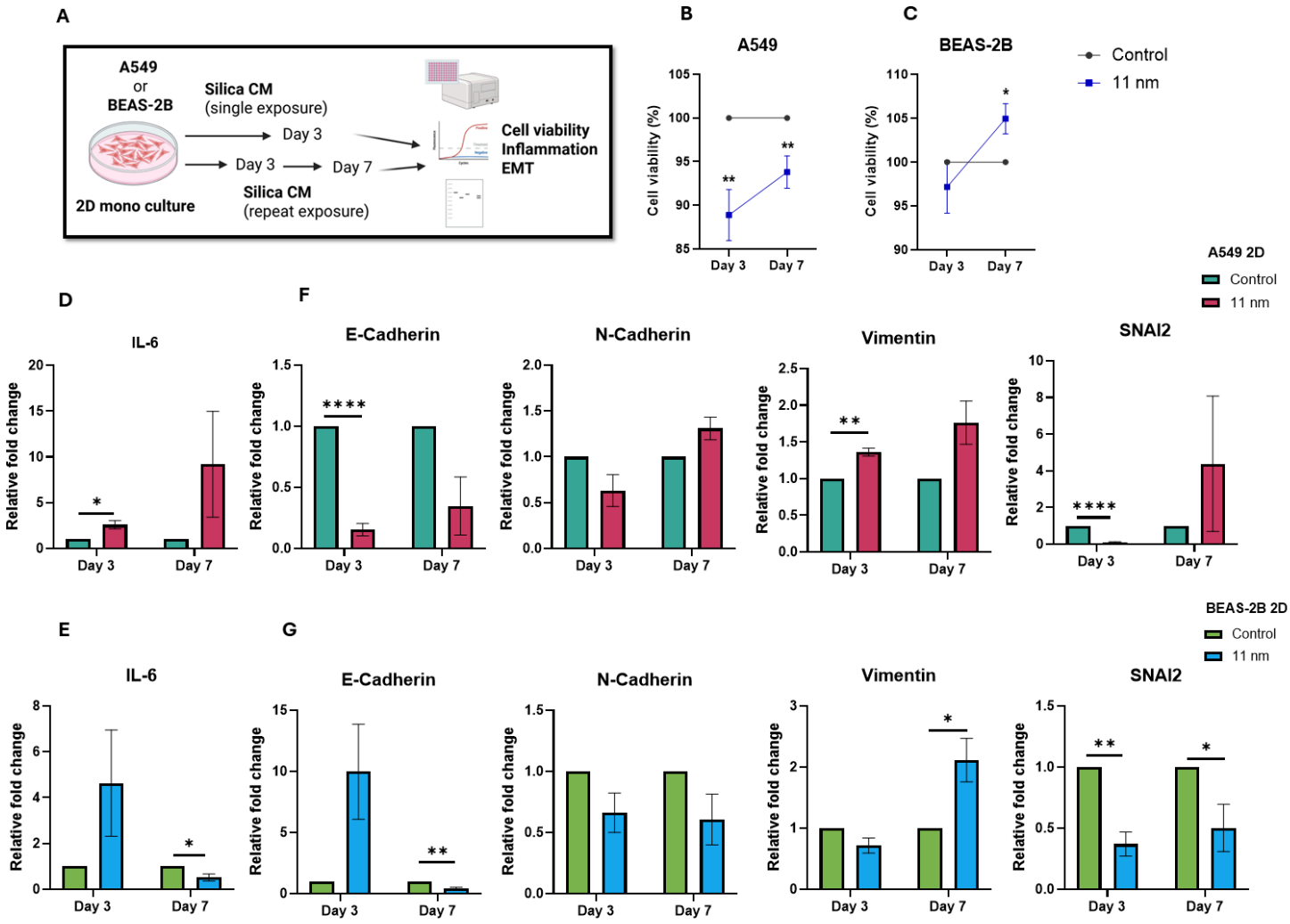


Figure 2

2D models of A549 and BEAS-2B show a differential profile upon exposure to silica CM

(**A**) Representation of workflow. Cell viability in a 2D model of (**B**) A549 and (**C**) BEAS-2B cells exposed to silica CM relative to control groups. mRNA expression of pro-inflammatory cytokine levels in (**D**) A549 and (**E**) BEAS-2B cells. Analysis of EMT markers in (**F**) A549 and (**G**) BEAS-2B cells by real-time PCR. Data represented as mean ± SEM (n = 3 to 6). *p < 0.05, **p < 0.01, ****p < 0.0001.

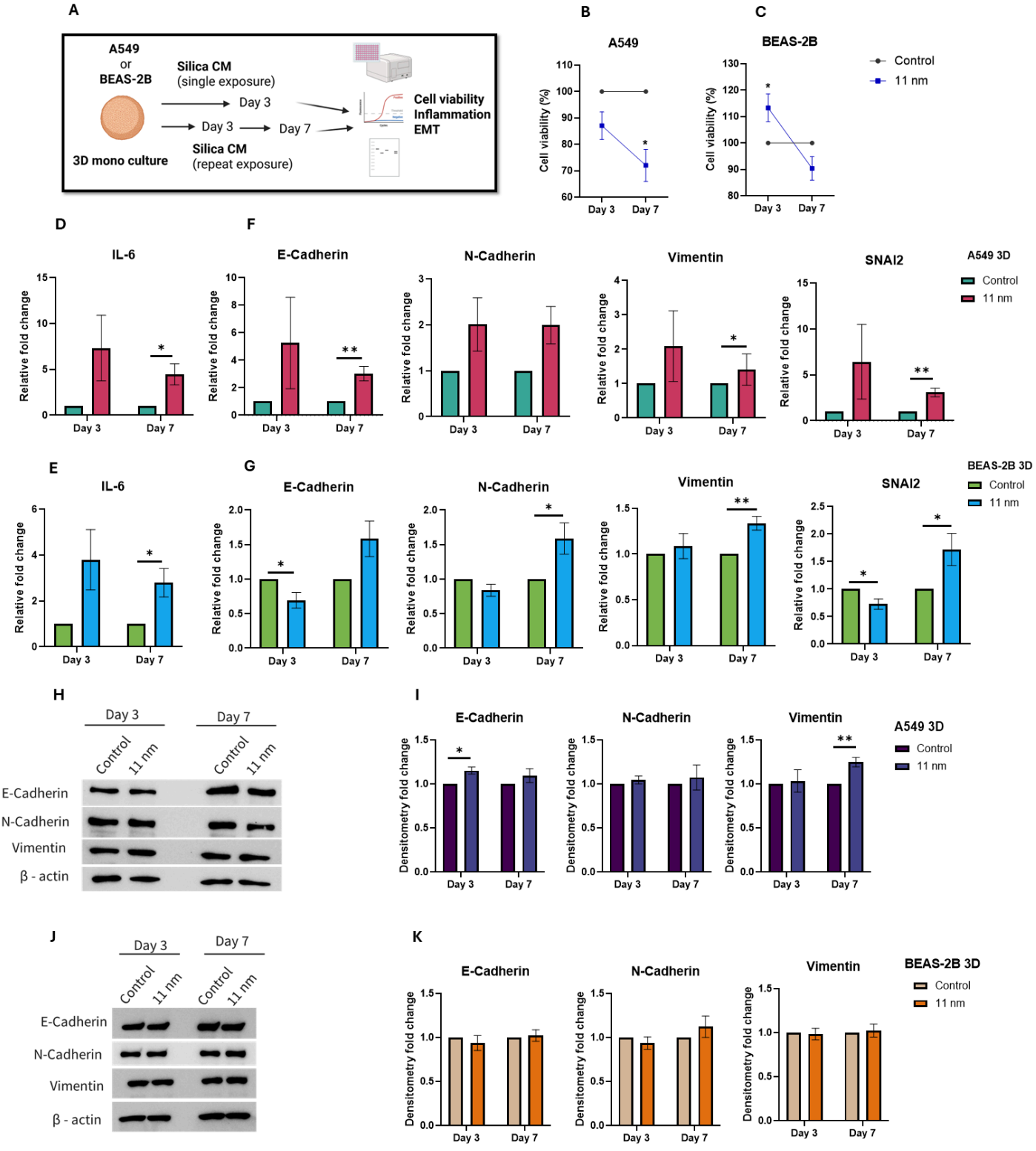


Figure 3

Silica CM induces an EMT phenotype in A549 3D spheroids

(**A**) Schematic representation of workflow. (**B**) A549 and (**C**) BEAS-2B cell viability of 3D spheroids upon exposure to silica CM. IL-6 mRNA levels in (**D**) A549 and (**E**) BEAS-2B by real-time PCR. mRNA levels of EMT markers in (**F**) A549 and (**G**) BEAS-2B cells. Protein expression and densitometry analysis of EMT

markers for (**H, I**) A549 and (**J, K**) BEAS-2B cells, respectively. All data are represented as mean ± SEM (n = 3 to 5). *p < 0.05, **p < 0.01.

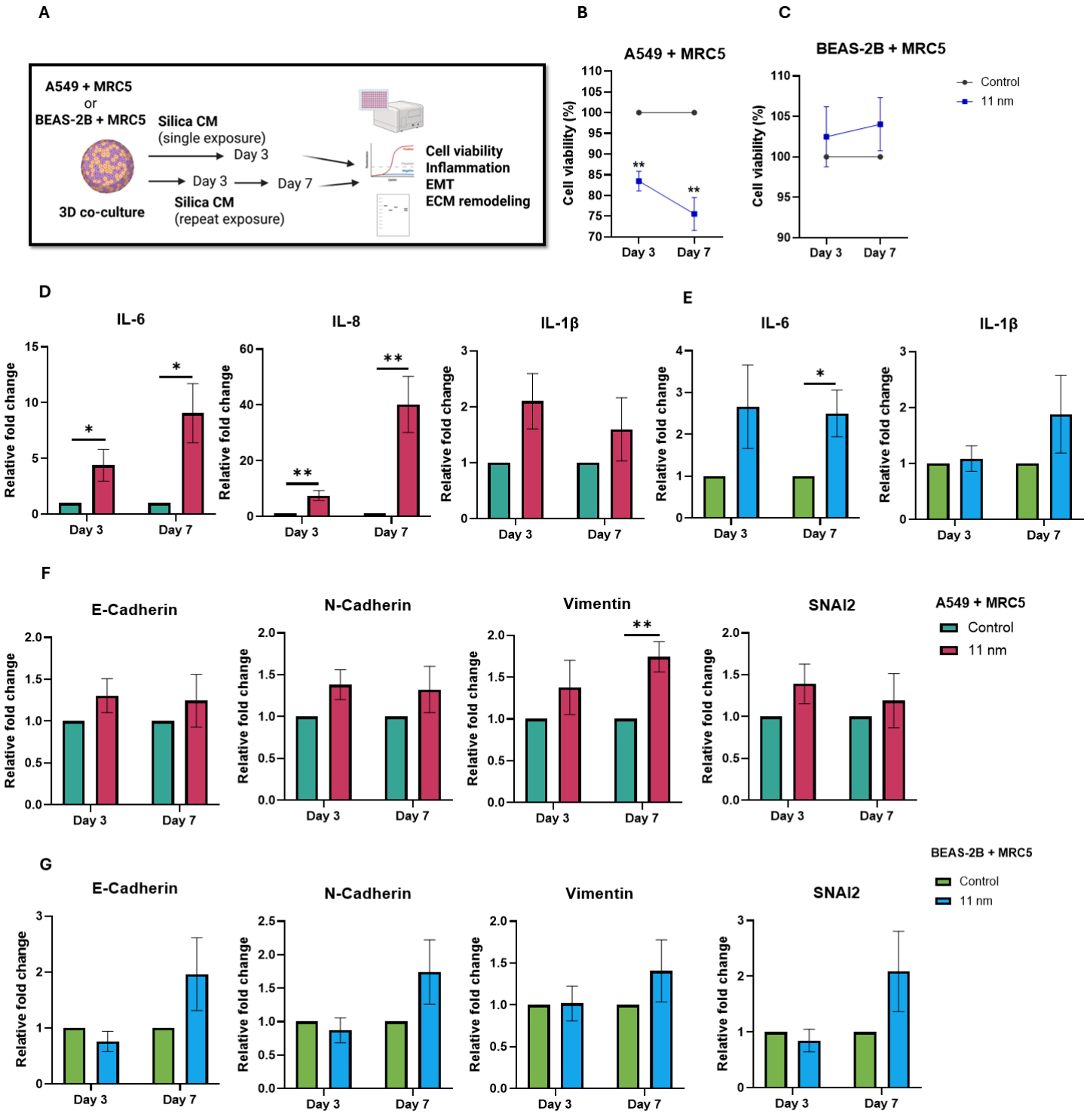


Figure 4

Silica CM triggers an inflammatory response in 3D co-culture spheroids

(**A**) Schematic workflow. Cell viability of (**B**) A549 and (**C**) BEAS-2B 3D spheroid during silica CM exposure when co-cultured with MRC5 fibroblasts. mRNA levels of inflammatory markers in (**D**) A549 and (**E**) BEAS-2B 3D co-culture spheroids by real-time PCR. mRNA expression levels of EMT markers in (**F**) A549 and (**G**) BEAS-2B 3D co-culture spheroids. Data represented as mean ± SEM (n = 3 to 6). *p < 0.05, **p < 0.01.

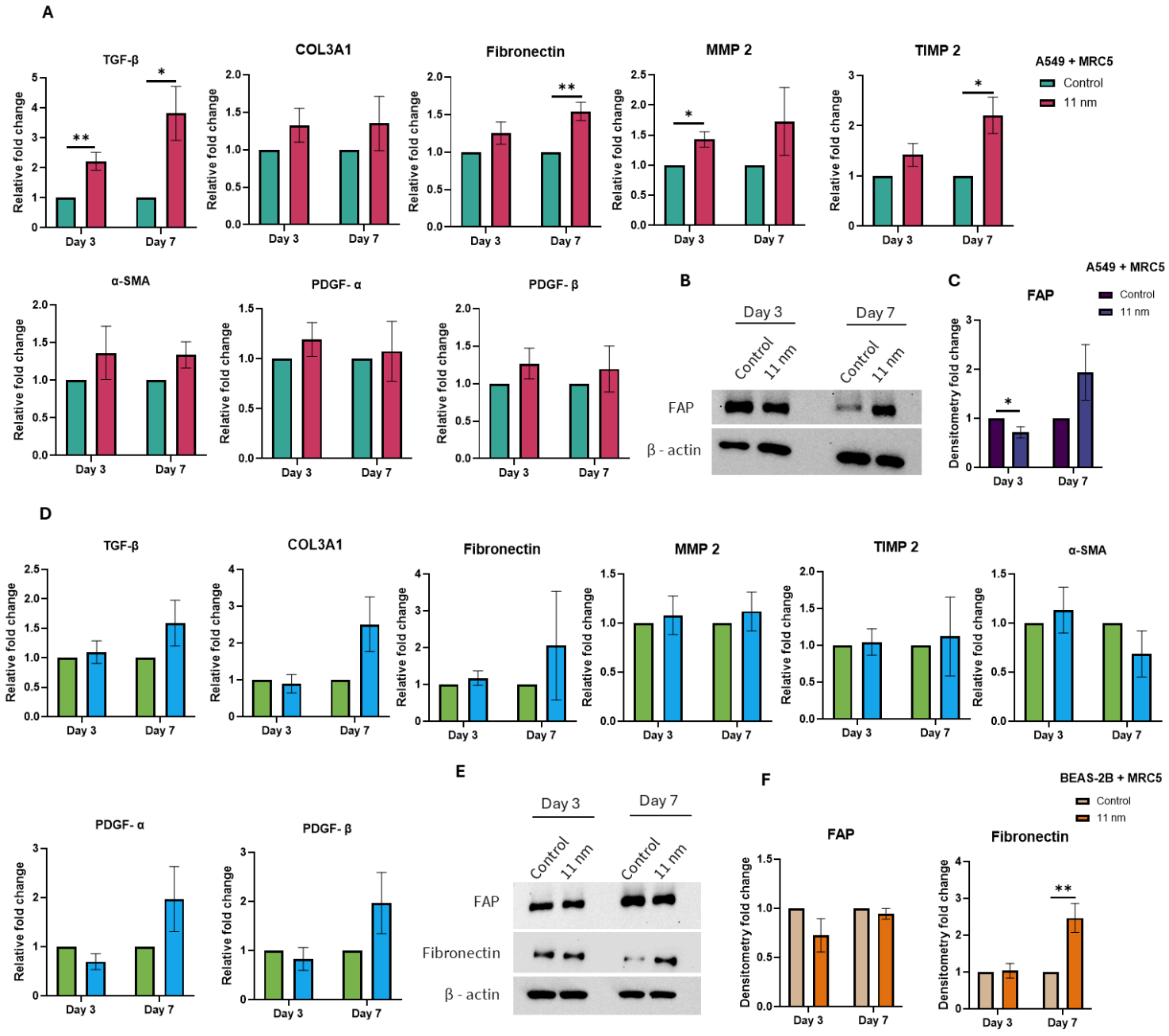


Figure 5

Differential profile of fibrogenesis and ECM remodeling in A549-MRC5 and BEAS-2B-MRC5 3D co-culture spheroids during silica CM treatment

mRNA levels of fibrotic and matrix remodeling associated markers in (**A**) A549 and (**D**) BEAS-2B 3D spheroids co-culture during silica CM exposure. Protein expression levels in (**B**) A549 and (**E**) BEAS-2B and their respective densitometry analysis (**C**) and (**F**). Data are represented as mean ± SEM (n = 4 to 6). *p < 0.05, **p < 0.01.

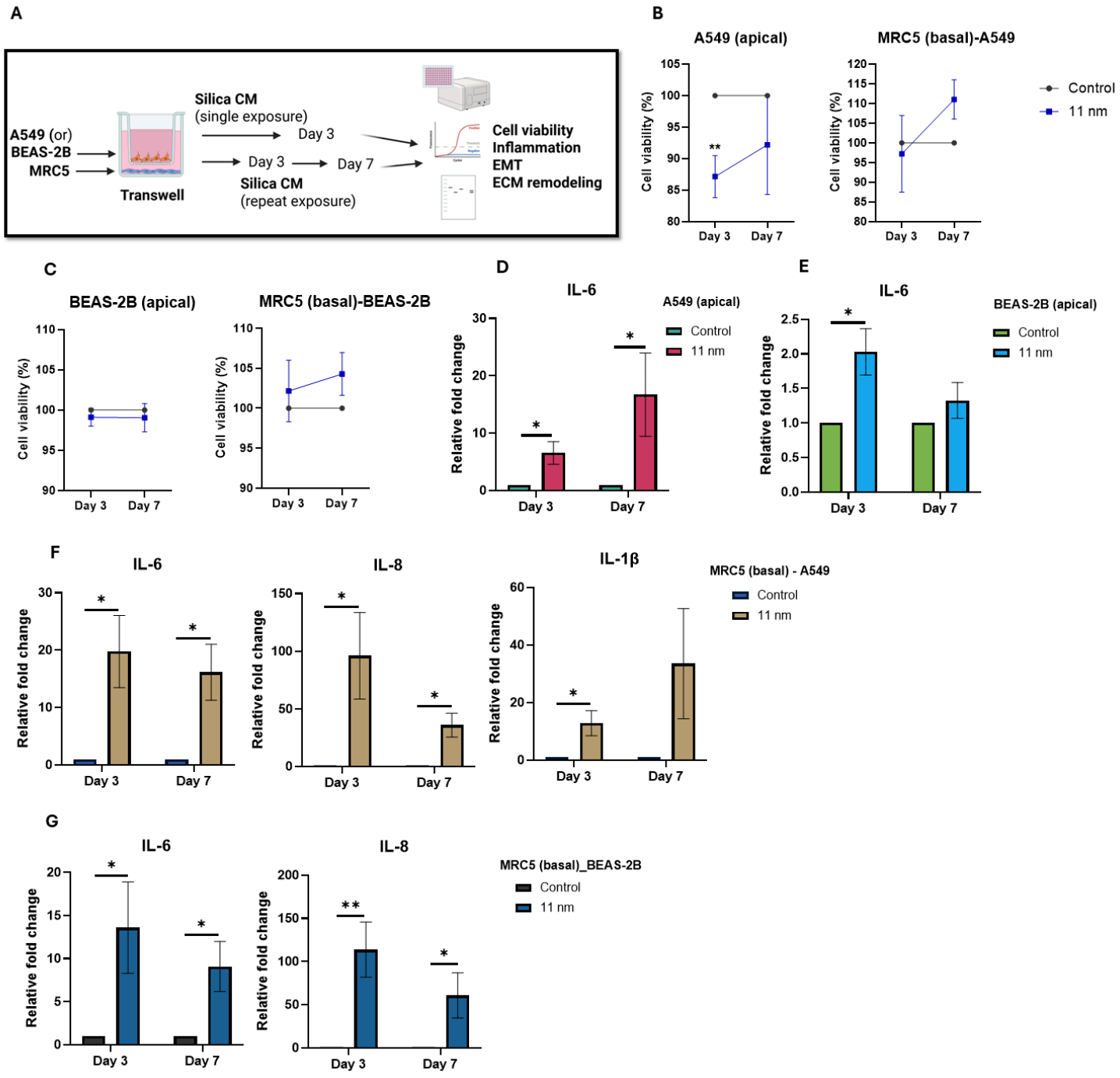


Figure 6

Silica CM induces inflammation in both epithelial and fibroblast transwell co-cultures

(**A**) Graphical representation of workflow. (**B**) A549 (apical) and (**C**) BEAS-2B (apical) cell viability along with their MRC5 (basal) when exposed to silica CM. IL-6 mRNA levels in (**D**) A549 (apical) and (**E**) BEAS-2B (apical) by real-time PCR. mRNA levels of inflammatory markers in (**F**) MRC5 (basal) - A549 and (**G**) MRC5 (basal) - BEAS-2B cells respectively. All data are presented as mean ± SEM (n = 4 to 6). *p < 0.05, **p < 0.01.

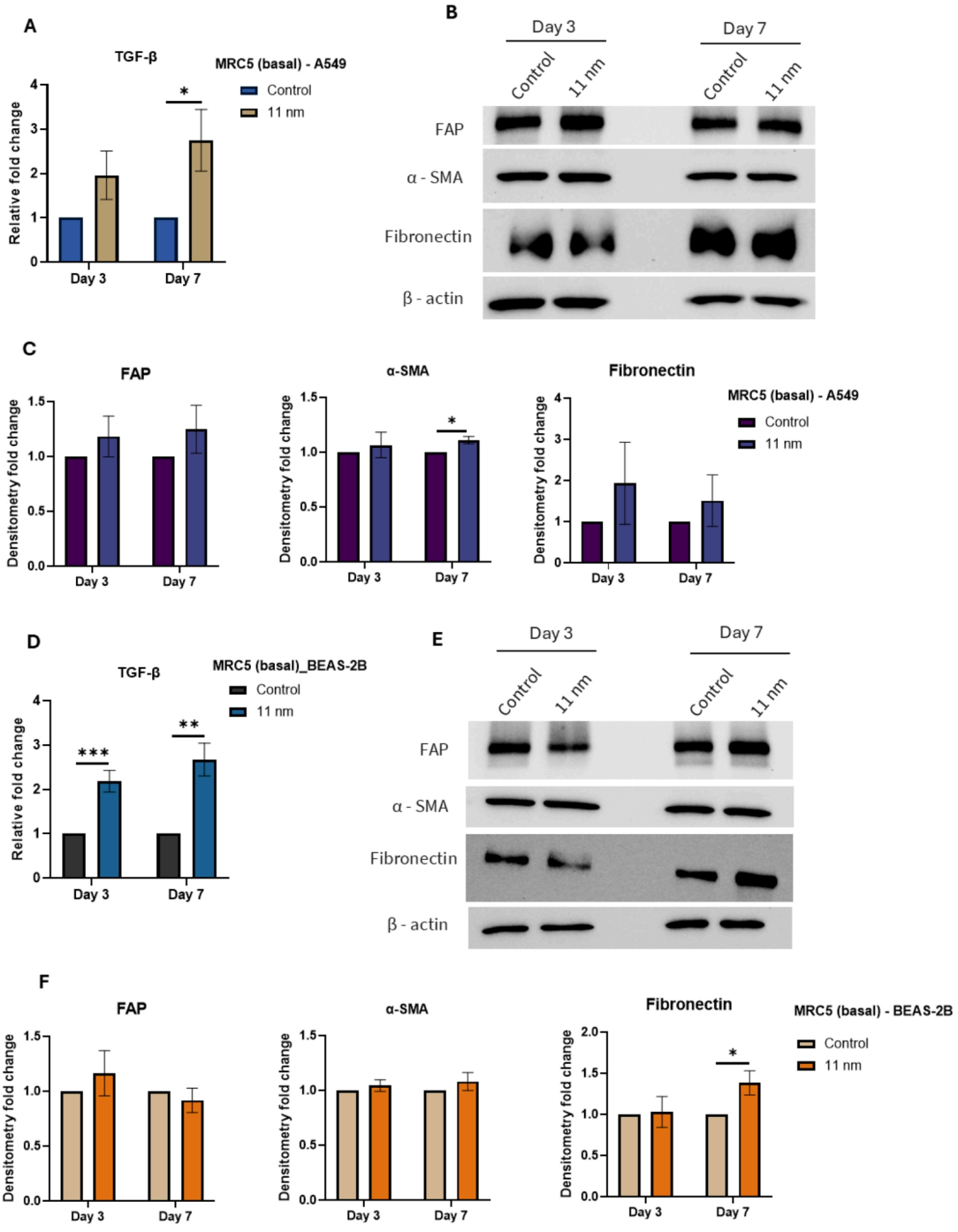


Figure 7

Silica CM triggers fibrogenesis in MRC5 transwell co-cultures with epithelial cells

mRNA levels of TGF-β in (**A**) MRC5 (basal) - A549 and (**D**) MRC5 (basal) - BEAS-2B co-cultures. Protein expression levels and their densitometry analysis of fibrogenesis and tissue remodeling markers in (**B, C**) MRC5 (basal) - A549 and (**E, F**) MRC5 (basal) - BEAS-2B cells, respectively. All data are presented as mean ± SEM (n = 4 to 6). *p < 0.05, **p < 0.01, ***p < 0.001.

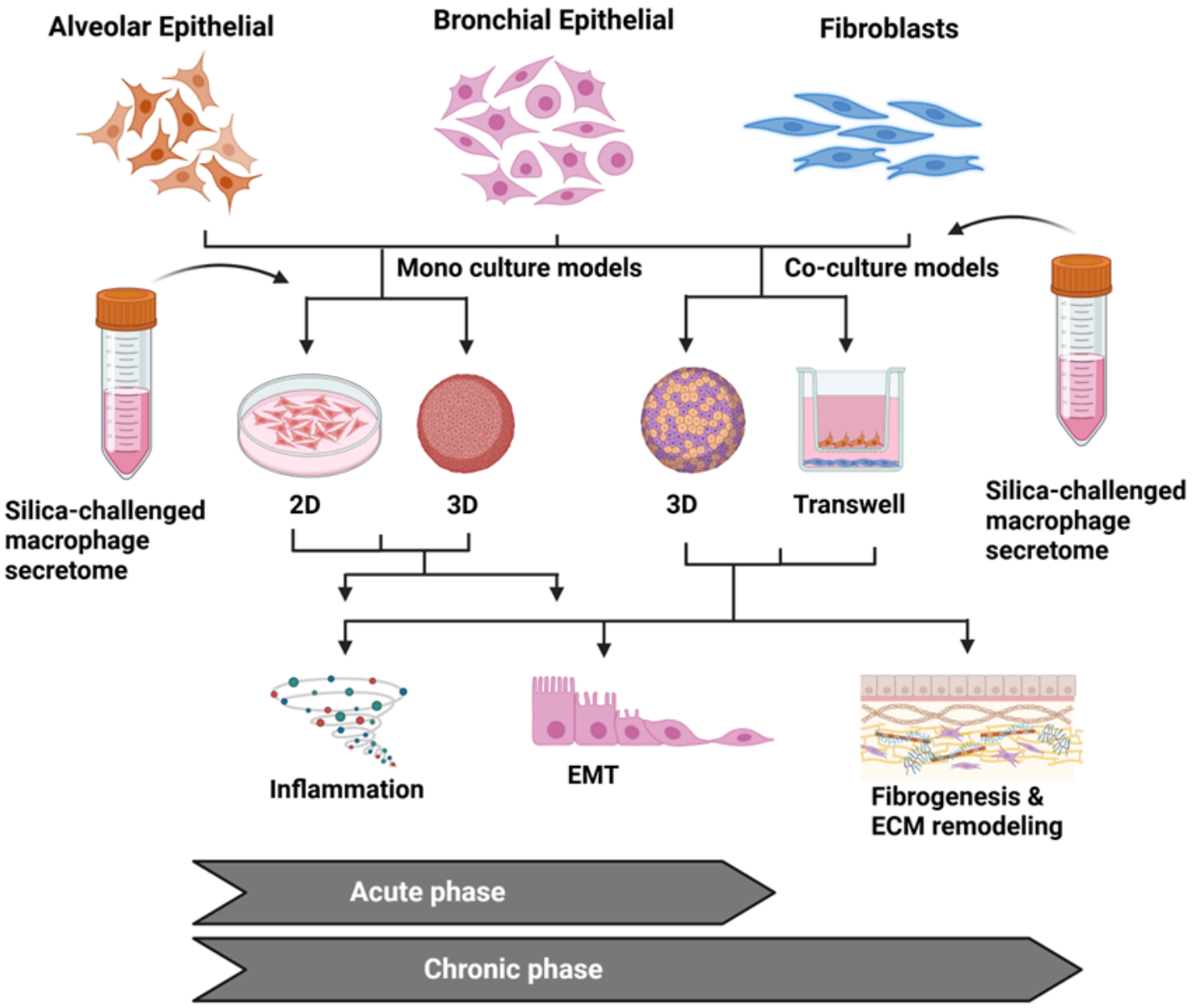


Figure 8

Graphical abstract of workflow summary

Supplementary Files

This is a list of supplementary files associated with this preprint. Click to download.

- SelvamaniSPetal2026SupplementaryFile.docx